Organic Electronics 12 (2011) 1483–1492

Contents lists available at ScienceDirect

Organic Electronics

journal homepage: www.elsevier.com/locate/orgel

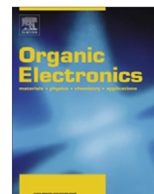

Electronic and magnetic properties of C_{60} thin films under ambient conditions: A multitechnique study

O. Amelines-Sarria [a], P.C. dos Santos Claro [b], P.L. Schilardi [b], B. Blum [b], A. Rubert [b], G. Benitez [b], V.A. Basiuk [a], A. González Orive [c], A. Hernández Creus [c], C. Díaz [b], R.C. Salvarezza [b,*]

[a] Instituto de Ciencias Nucleares, Universidad Nacional Autónoma de México, Circuito Exterior, C.U., 04510 México D.F., Mexico
[b] Instituto de Investigaciones Fisicoquímicas Teóricas y Aplicadas (INIFTA), Facultad de Ciencias Exactas, Universidad Nacional de La Plata, CONICET, Sucursal 4 Casilla de Correo 16, 1900 La Plata, Argentina
[c] Departamento de Química Física, Instituto Universitario de Materiales y Nanotecnología, Astrofísico F. Sánchez s/n, 38205 La Laguna, Tenerife, Canary Islands, Spain

ARTICLE INFO

Article history:
Received 19 March 2011
Received in revised form 6 May 2011
Accepted 25 May 2011
Available online 12 June 2011

Keywords:
Fullerenes
Thin films
Magnetic properties
Electronics properties
Ambient conditions

ABSTRACT

The magnetic and electronic properties of thin C_{60} films (film thickness $\geqslant$4 ML) grown by sublimation in vacuum on oxidized Si, Au, highly oriented pyrolytic graphite and glass, and subsequently exposed to ambient conditions, are investigated by using a multitechnique approach. The films exhibit a structure consisting of nanometric aggregates, whose size increases with film thickness, irrespective of the substrate, although larger aggregates are found on Au substrates. The XPS data indicate no significant degradation of the C_{60} films, even though significant amounts of oxygen are present. Magnetic properties are characteristic of C_{60} films exposed to oxygen and light. In contrast, STS measurements show that the local electronic properties are similar to those reported for ultrathin films grown on the same substrates under vacuum. A detailed discussion on the effects of film-thickness and substrate-type on the C_{60} film properties, under ambient conditions, is presented.

© 2011 Elsevier B.V. All rights reserved.

1. Introduction

Since their discovery [1] and the beginning of massive production [2], fullerenes and their derivatives have received great attention. One of the main reasons is that they offer many new applications in science and technology, as building blocks for cluster assembled materials with specific tailored properties [3], in organic photovoltaic devices [4], as substrates for adhesion of bone cells [5], and growth of diamond [6] or silicon carbide films [7]. C_{60} films grown on different types of surfaces have potential applications as chemical sensors [8–11], superconductors [12] and single-molecule transistors [13].

The adsorption of C_{60} onto semiconductor [14–20] and metallic [21–25] surfaces was intensively studied during the 90s, primarily under UHV conditions, for crystallographically characterized substrates and very thin films, i.e., far from normal working and ambient conditions. Silicon surfaces have been most studied among semiconductors, due to their scientific importance in such fields as optoelectronic devices and solar cells [4]. However, the nature of the bonding between C_{60} and Si surfaces shows contradictory results, indicating either C_{60} physisorption [19,26] or chemisorption [15,18], or both simultaneously [27]. The electronic structure of fullerene films grown on SiO_x/Si(1 0 0) obtained by photoemission indicates that the SiO_x/Si surface is non-reactive with respect to the interaction with C_{60}. Gold has been among the most studied metallic surfaces for thin C_{60} films. There are reports indicating that the charge transfer from metal to C_{60} is higher than that produced by semiconductor surfaces

* Corresponding author. Tel.: +54 221 4257430; fax: +54 221 4254642.
E-mail address: robsalva@inifta.unlp.edu.ar (R.C. Salvarezza).
URL: http://nano.quimica.unlp.edu.ar (R.C. Salvarezza).

1566-1199/$ - see front matter © 2011 Elsevier B.V. All rights reserved.
doi:10.1016/j.orgel.2011.05.024

[25]. Therefore, the general belief is that interaction between C_{60} and noble metal surfaces has an ionic character. However, Wang and Cheng reported that this interaction is covalent with some ionic features [28]. By comparison, there are far less studies for C_{60} evaporated onto HOPG [29–32]. Only one of them investigates the nature of the C_{60}-substrate interaction, and finds that C_{60} adsorbs on HOPG by van der Waals interactions [30].

Scanning tunneling spectroscopy (STS) is a unique technique that allows a direct measure of the local density of states (DOS) near the Fermi energy. In order to study the electronic structure, STS has been performed on thin films of C_{60} deposited by sublimation onto different substrates and changes in HOMO, LUMO and HOMO–LUMO gaps are studied. These values have been reported for single C_{60} molecules and ultrathin C_{60} films (thickness < 1 ML) on Si [25,33–35], Au [17,36–40] and HOPG [41], for different adsorption sites and surface conformations. The overall tendency is that the gap values for C_{60} on Si are smaller (*ca.* 1.7 eV) than those obtained on Au surfaces (*ca.* 2.55 ± 0.25 eV), due to charge transfer from Au to the C_{60} molecules.

In contrast to the large amount of literature concerning the C_{60} electronic properties at submonolayer or monolayer coverages, less attention has been paid to these properties for C_{60} films on Si, Au and HOPG at coverages above 4 ML. There is even less information on the electronic properties of thin C_{60} films exposed to ambient conditions, despite the fact that in many cases manipulation and applications of these films are performed under light and atmospheric oxygen levels. It is known that under these conditions, changes in macroscopic physical and chemical properties of C_{60} films take place [17,42–45]. For example, exposure to light and oxygen induces changes in the C_{60} films from diamagnetic to ferromagnetic [45]. Light and oxygen exposure of these films can also affect the electronic properties of these films [46–49]. Therefore, further knowledge on their electronic properties under these conditions is a key point for predicting their performance under normal ambient conditions, and could affect many technological developments.

In this paper, we present a study on the magnetic and electronic properties of C_{60} thin films (film thickness $\geqslant$ 4 ML) sublimated onto naturally oxidized Si(1 0 0), Au films, glass, and HOPG surfaces exposed to ambient conditions. The films are characterized by atomic force microscopy (AFM) and X-ray photoelectron spectroscopy (XPS) while magnetic and electronic properties are studied by magnetic force microscopy (MFM) and scanning tunneling spectroscopy (STS), respectively. In particular we estimate for the first time the gap energies for the above mentioned thin films allowing a direct comparison with the values reported at lower coverages and under vacuum conditions. We have also determined the influence of the substrate and thickness of the films on their morphology, electronic structure and adhesion strength/wear resistance. This article is organized as follows: first we explore the structure of the films by AFM, then, we characterize the systems by XPS and MFM, and finally we explore their electronic structure by STS.

2. Experimental

Fullerene films were grown by sublimation of C_{60} (Sigma–Aldrich Company, USA, 99.5%) on clean Au films deposited onto glass (250 nm gold thickness, Arrandees™), freshly cleaved highly oriented pyrolytic graphite (HOPG), naturally oxidized Si(1 0 0) surfaces and glass. An Edwards 360 metal coater operating at 10^{-6} Torr was used for the deposition. Films were simultaneously prepared on all four kinds of substrates mounted at the same distance and geometry from the C_{60} source, in single evaporation experiments, to assure similar preparation conditions at each given film thickness. The films were then stored in ambient conditions for several days and finally cleaned under nitrogen flux immediately before characterization.

Film morphology was characterized by imaging the samples with an atomic force microscope (Nanoscope IIIa, Digital Instrument/Veeco) operating in the contact mode, with silicon nitride tips. The chemical composition of the films and the nature of the chemical bonds of the species present were corroborated by X-ray photoelectron spectroscopy (XPS). Photoelectrons were excited with a Mg Kα source (XR50, Specs GmbH) and detected with a hemispherical electron energy analyzer (PHOIBOS 100, Specs GmbH). A two-point calibration of the energy scale was performed using sputter-cleaned gold (Au $4f_{7/2}$, binding energy BE = 84.00 eV) and copper (Cu $2p_{3/2}$, BE = 933.67 eV) foils.

Electronic properties of the films were determined by STS measurements using a scanning tunneling microscope (Nanoscope IIIa, Digital Instruments/Veeco) operating in air at room temperature. Pt–Ir tips were used for these measurements. The tunneling current vs bias voltage (I vs V) curves were averaged over at least three different regions of the samples. The dI/dV plots shown in this paper are the average of ten measurements. These measurements were taken under the same experimental conditions, but performed on different regions of each sample. Smoothening of the dI/dV plots was performed by using the Savitzky–Golay differentiation [50].

Film thickness was determined by AFM measurements of films grown by stencil lithography patterning through a hexagonal mask, in parallel with the other C_{60} films. The height difference between the masked and the exposed regions has been taken as a measure of the film thickness of the set of samples grown under the same experimental conditions, taking into account that once the film has nucleated, film thickness growth, on average, proceeds independent of the substrate employed [51].

Magnetic force gradient (MFM) and topographic sample images were obtained simultaneously with a NanoScope IIIa scanning probe microscope (Digital Instruments/Veeco) at room temperature in air. The microscope was operated in the tapping/lift™ scanning mode, i.e., the AFM tip was made to scan the sample at different heights above the topographic height of the sample at each point in order to separate short range topographic effects from long range magnetic signals. Lift-heights ranging from 25 to 100 nm were selected. Images were taken at a scanning rate of 1 Hz using a MESP (60–100 kHz, 1–5 N/m) scanning probe

coated with a magnetic CoCr alloy thin film. In addition, silicon FESP tips with the same range of frequency, force constant and dimensions, but uncovered (non magnetic) were used to compare the contrast phase signal obtained with both tips at different heights of the sample. This procedure was also applied with the bare substrates. Prior to acquiring images, the tips were exposed to a 0.3 T magnetic field.

3. Results and discussion

3.1. AFM characterization

Fig. 1 shows AFM images of C_{60} films of different thickness (h); that were grown by sublimation on the native SiO_x substrates. AFM images show that the films are formed by nanometric aggregates that entirely cover the SiO_x surface.

The average size (d) of the aggregates increases from ≈20 to ≈70 nm as h is increased from 3 nm (≈4 monolayers) to 70 nm (≈100 monolayers) and remains constant for thicker films, as determined by power spectral density analyses (right panel in Fig. 1). The mean square roughness (Rq) corresponding to the films with h of 3, 40, 70 and 100 nm are 1.06, 1.13, 2.75 and 3.46 nm, respectively.

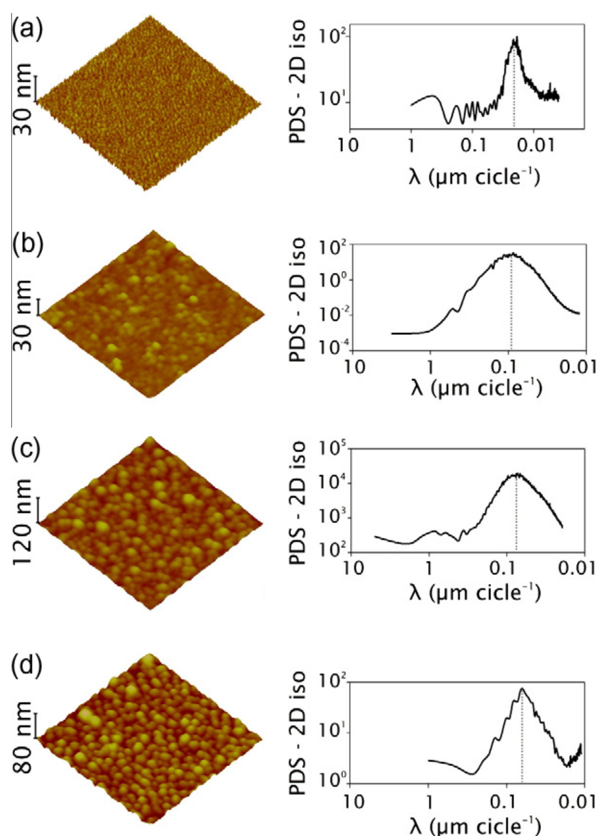

Fig. 1. Left: three-dimensional AFM images (1 × 1 μm^2, contact mode) of C_{60} films with different thickness (h) on silicon oxide substrates. Right: power spectral density (PSD) data corresponding to the AFM images on the left, after high-pass filtering. The grey lines indicate the average grain size (d). (a) h = 3 nm and d = 19 nm. (b) h = 40 nm and d = 55 nm. (c) h = 70 nm and d = 74 nm. (d) h = 100 nm and d = 60 nm.

Comparing h and Rq for each film, we note that for thin films (h = 3 nm) the roughness is 35.3% of the total film thickness, that is, the film topographical morphology is very irregular. On the other hand, the roughness parameter for the films with h of 40, 70 and 100 nm is 2.8%, 3.9% and 3.5% of the film thickness, respectively, which suggests a high degree of smoothness.

We observe that the films with h > 70 nm exhibit good adherence to the substrates, remaining stable under repetitive scanning with the AFM tip in the contact mode. In contrast, the adherence and wear resistance are poor for films with h = 3 nm, where repetitive scans with the tip finally open a window. In the irregular morphology present in the 3 nm thick films we expect that the outer C_{60} molecules exhibit weak van der Waals interactions so that the outer layer can be easily removed by the AFM tip. On the contrary, thicker films consist of large clusters where one expects stronger molecular interactions, and accordingly, the C_{60} molecules remain stable under tip scanning. We also note that the variations in the film thickness is accompanied by a change in the sample color from a pale brown (h = 3 nm) to green–blue (h > 40 nm). As we will see later, this color change is not related to the gap value and is mainly due to a light interference phenomenon.

Each film thickness was estimated by stencil lithography of a sample prepared in parallel with the continuous films (Fig. 2a). The height difference between the masked and exposed regions (Fig. 2b) has been taken as a measure of the film thickness for the set of samples grown during the same C_{60} sublimation experiment.

Fig. 3 shows high-pass filtered images for films of similar thicknesses grown in different sublimations on oxidized Si, HOPG, Au and glass. The images reveal a similar aggregate morphology irrespective of the substrate, but in the films grown on Au, the size of aggregates and the channels separating them are larger than on other substrates. While the high-pass filtered images allow a direct and easy comparison of the aggregate size, it loses the z-component of the image. The conventional top-view images in Fig. 4 illustrate the difference in film structure providing also information in the z-direction. Here we show C_{60} films prepared simultaneously in the same evaporation chamber on oxidized Si (Fig. 4a) and Au (Fig. 4b), both with a thickness of h ≈ 30 nm. The images not only reveal larger aggregates for the C_{60} film grown on Au, but

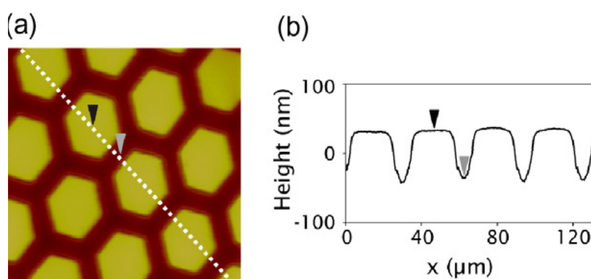

Fig. 2. (a) AFM image (2D view, 1 × 1 μm^2) of a patterned C_{60} film on SiO_x/Si. (b) Cross section profile across the dashed line in (a); the height difference between the black and grey arrows is h = 70 nm.

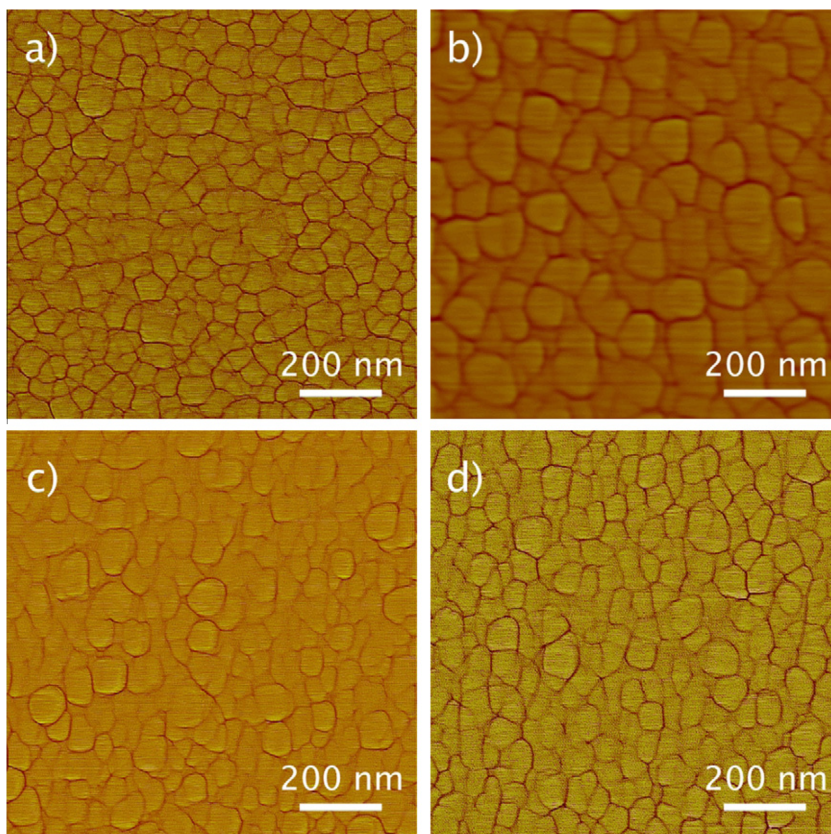

Fig. 3. AFM images (2D view, high pass filtered, 1 × 1 μm^2) of C_{60} films grown in different sublimations on different substrates. (a) Si, h = 100 nm, (b) Au, h = 140 nm, (c) HOPG h = 80 nm, (d) glass, h = 100 nm.

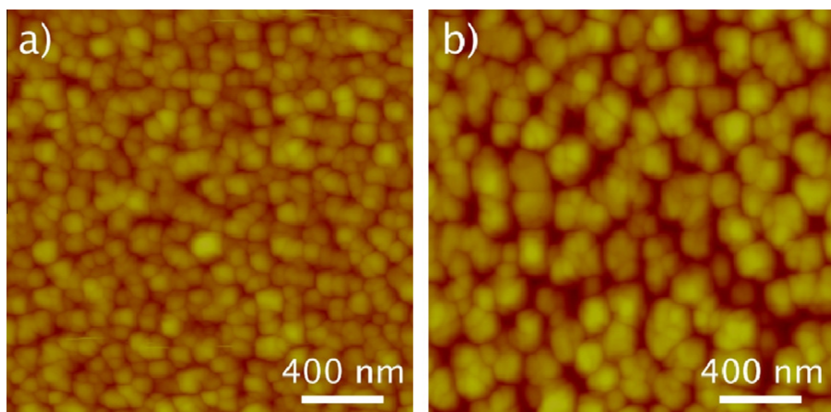

Fig. 4. AFM images (2D view, 2 × 2 μm^2) of C_{60} films (h = 30 nm) prepared simultaneously on (a) oxidized Si(1 0 0) and (b) Au.

also a smaller connectivity between them, since they are separated by wider and deeper channels. The difference between aggregate size in Fig. 4, can be explained if we consider that, for submonolayer coverages, the C_{60} molecules have higher mobility on Au, facilitating the formation of large islands [21] and trenches, in contrast to what happens to the films grown on SiO_x, HOPG or glass where the first C_{60} molecules are isolated and dispersed on the surfaces, forming many more cluster seeds [15,52]. As a result, at higher coverages, the films grown on Au show larger clusters than those obtained on the others substrates (SiO_x, HOPG and glass).

3.2. XPS data

The XPS data for C_{60} films deposited onto SiO_x (h = 70 nm) are presented in Fig. 5. The survey spectrum (Fig. 5a) exhibits a strong C signal. Some O and only small

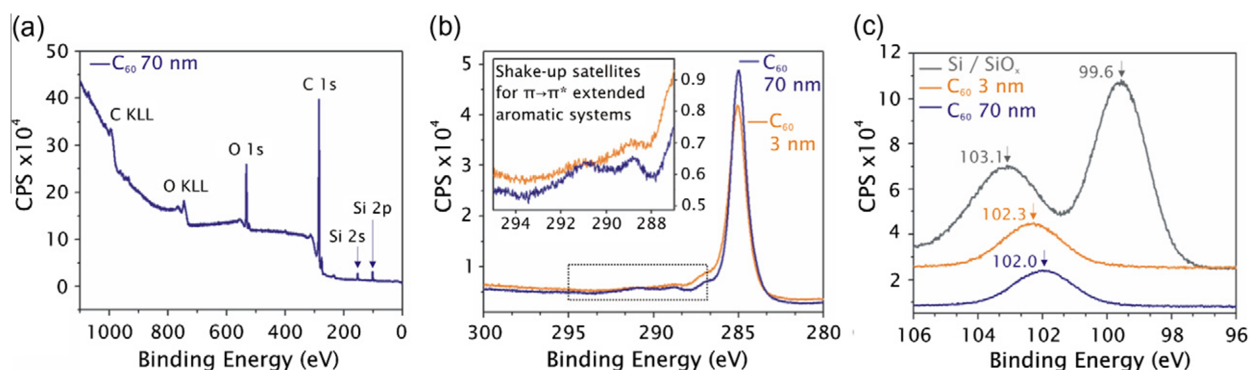

Fig. 5. XPS data for C_{60} films on oxidized silicon support: (a) survey spectrum (70-nm film), (b) C 1s spectra for 3 nm (orange) and 70 nm (blue) thick C_{60} films. Inset shows shake-up satellites attributable to C_{60} presence (c). Comparison Si 2p region between the same two C_{60} films and a SiO_x/Si reference (grey curve). C_{60} films interact with silicon substrate and show a kind of SiO_xC_y species (102.2 ± 0.1 eV) [56]. (For interpretation of the references to colour in this figure legend, the reader is referred to the web version of this article.)

amounts of Si are detected, in agreement with the film thickness and morphology (almost complete coverage of SiO_x by C_{60}) as determined by AFM. The atomic ratio between O and Si is roughly 4:1. The excess O can be associated with the extreme reactivity of C_{60} crystals to (atmospheric) oxygen [53], which quickly penetrates into the bulk fullerene. No traces of metallic contaminants can be observed in the spectra.

Fig. 5b shows XPS spectra of C 1s core level and shake-up satellites (inset in Fig. 5b) for C_{60} with film thicknesses of 3 nm (orange)[1] and 70 nm (blue),[1] and a large peak at 285 eV, typical for C_{60} films. The absence of components at energies below 283 eV is indicative of the lack of Si–C bonding in the films [17,25,54]. The inset in Fig. 5b illustrates the expanded region covering the C1s shake-up satellites. We resolved by high-resolution photoelectron spectroscopy two peaks for the deposited C_{60} film at 3.7 and 6 eV relative to the C1*s* binding energy; these results are consistent with two of the four peaks obtained in the report by Enkvist [55]. This result indicates that no significant degradation of the C_{60} films takes places under our experimental conditions.

Fig. 5c shows XPS spectra of the Si 2p core level region for a SiO_x/Si reference surface and C_{60} films of 3 and 70 nm thickness on SiO_x/Si(1 0 0). For the reference surface, two peaks are seen at 99.6 and 103.1 eV corresponding to Si^0 (Si–Si) and Si^{+4} (SiO), respectively. For the fullerene films, only one peak is found at 102.3 eV (3 nm film) or 102.0 eV (70 nm film) corresponding to Si^{+3}. By analogy with reports on oxidation of SiC [56], we can conclude that the SiO_x–C_{60} interface is mainly composed by SiO_xC_y.

3.3. MFM characterization

MFM was used to characterize magnetic properties of the C_{60} films. In order to enhance the magnetic contrast we used hexagonally patterned C_{60} films prepared by stencil lithography, as shown in Fig. 2. In Fig. 6 we show the topographic image (a) and magnetic phase contrast (b) of these films on glass. Magnetic contrast concentrated on the hexagons is evident in the C_{60} film as shown in Fig. 6b. On the other hand, the same experiments (Fig. 6c–d) under identical imaging conditions but using a non-magnetic tip give no evidence of the hexagons in the phase contrast magnetic image (Fig. 6d). Similar results are obtained for the C_{60} films deposited on the different substrates used in this work. Therefore, the MFM characterization indicates that our films are magnetic. While pristine van der Waals C_{60} crystals are diamagnetic, this behavior changes when the sample is exposed to oxygen under the action of the visible light [17]. These conditions apply to our films exposed to light under atmospheric conditions, since they contain excess amounts of oxygen as shown in the XPS data (Fig. 5a). It is known that light exposure during 2.5 h brings noticeable features of ferromagnetism: non-linear magnetization process at low fields and magnetization increases related to an increase in the exposure time [42,53].

The MFM images at high resolution (insets in Fig. 6a–b) show that the magnetic field corresponds closely to the C_{60} aggregates present on the glass substrate. However, a detailed analysis of these images indicates that the magnetic contrast does not directly map onto the aggregates, consistent with locally induced polymerization of C_{60} films [45]. After having verified that our films exhibit the ferromagnetic behavior expected for C_{60} exposed to oxygen and light we will characterize their electronic properties and discuss them in relation to previous work obtained under UHV conditions.

3.4. STS: electronic properties

Typical curves of tunneling current vs. bias voltage for C_{60} films prepared on three different substrates are shown in Fig. 7. We used metallic (Au), semi-metallic (HOPG) and semiconductor (oxidized Si) substrates in order to gain insight on the influence of the substrate on the electronic structure of C_{60} films on materials with different bulk electronic properties. As a way to calibrate our STS measurements, we first measured the averaged *I/V* curves for the bare substrates (Fig. 7, left panels). The *I/V* curve for Au shows an almost linear behavior,

[1] For interpretation of the references to colour in this figure, the reader is referred to the web version of this article.

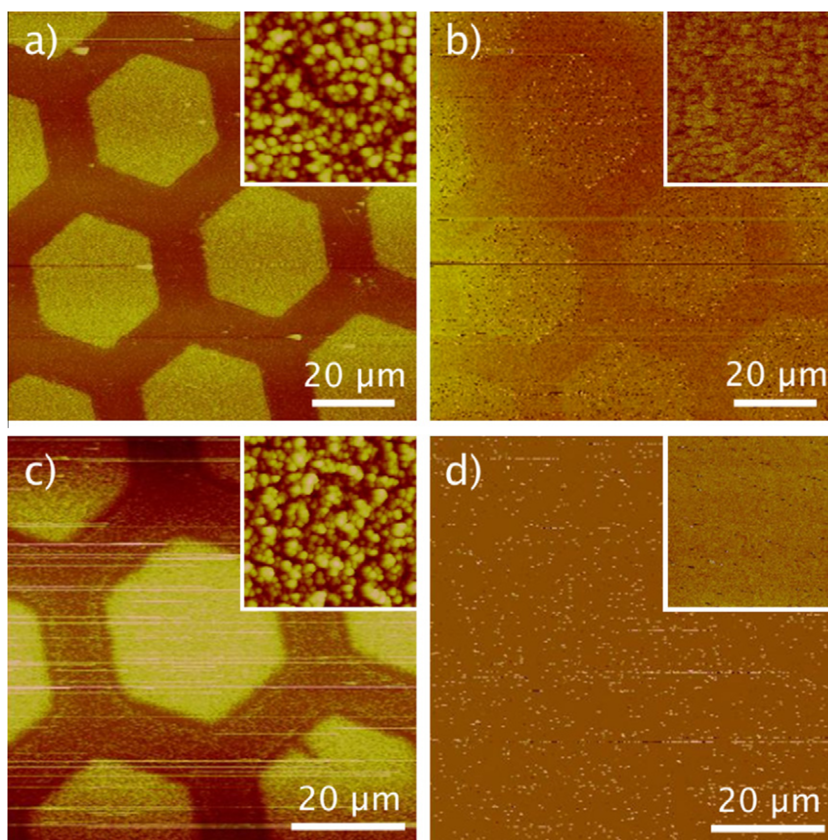

Fig. 6. (a and b) MFM images of patterned C_{60} films on glass. (a) Topographic image, $100 \times 100\ \mu m^2$; inset: detail of the hexagon ($3 \times 3\ \mu m^2$) (b) magnetic phase contrast, 25 nm lift scan height, $100 \times 100\ \mu m^2$; inset: detail of the hexagon ($3 \times 3\ \mu m^2$). (c and d) AFM images of patterned C_{60} films on glass. (c) Topographic image, tapping mode, $72.7 \times 72.7\ \mu m^2$; inset: detail of the hexagon ($3 \times 3\ \mu m^2$). (d) Phase contrast, 25 nm lift scan height, $72.7 \times 72.7\ \mu m^2$; inset: detail of the hexagon ($3 \times 3\ \mu m^2$).

as expected for metallic conductors [57]. In contrast, those recorded for SiO_x/Si(1 0 0) show zero current near the Fermi level, typical of semiconductors [58]. Meanwhile, the observed behavior for HOPG is intermediate between Au and SiO_x/Si(1 0 0). On the other hand, all *I*/*V* curves for the C_{60} films (Fig. 7, right panels) exhibit a response characteristic of semiconductor materials. Comparing the curves on the left of Fig. 7 with the curves on the right, it is clear that C_{60} masks the electronic properties of the pristine sample surfaces. For Au and HOPG, the change is very dramatic, while for SiO_x/Si(1 0 0) the only difference is that the width in the zero current response is greater for C_{60}/SiO_x/Si(1 0 0) than for SiO_x/Si(1 0 0), thus suggesting that the gap for the C_{60} film is larger than the corresponding for pristine support. The main difference observed between the three curves on the right is that the width of the linear response current region is greater for C_{60}/Au than for either C_{60}/HOPG or C_{60}/SiO_x/Si, which suggests that the gap width for the C_{60} film evaporated onto Au is higher than on either SiO_x or HOPG. While this same trend is observed for ultrathin C_{60} films (thickness < 1 ML) in UHV, where the gap is larger on Au [17,36–40] than on either Si [25,33–35], or HOPG [41]), it is very unlikely that STS can detect charge transfer from the substrate to films several layers high.

A better indication of the electronic state of a sample-surface and charge transfer processes involved can be obtained from the derivative tunneling spectra, *dI*/*dV*, (Fig. 8) which is a measure of the local density of states (LDOS) of a surface [59]. Our main objective was to quantify and compare the gap for all the fullerene films. The averaged derivative STS spectra for Au, HOPG and SiO_x/Si(1 0 0) were obtained at constant sample-tip separation conditions given by sample biases of 1.0, 0.5 and 2.0 V, respectively and a current of 1.0 nA.

The spectrum for Au (Fig. 8a) shows the expected metallic behavior, with a little curvature close to the Fermi level. On the other hand, the spectrum for HOGP (Fig. 8b) shows a slightly asymmetric parabolic shape of LDOS around the Fermi level as already reported for HOPG conductance data in ambient conditions [60,61].

Moreover, the spectrum for SiO_x/Si(1 0 0) exhibits a semiconductor behavior with a gap of 1.0 ± 0.1 eV. It shows good agreement with the values obtained in Refs. [62,63] and indicates that the average SiO_x thickness is at least 0.2 nm [62]. Our results are consistent with those reported in the literature, thus indicating that the ambient experimental conditions employed (open air and room temperature) are not responsible for the variations measured between bare and C_{60}-covered surfaces.

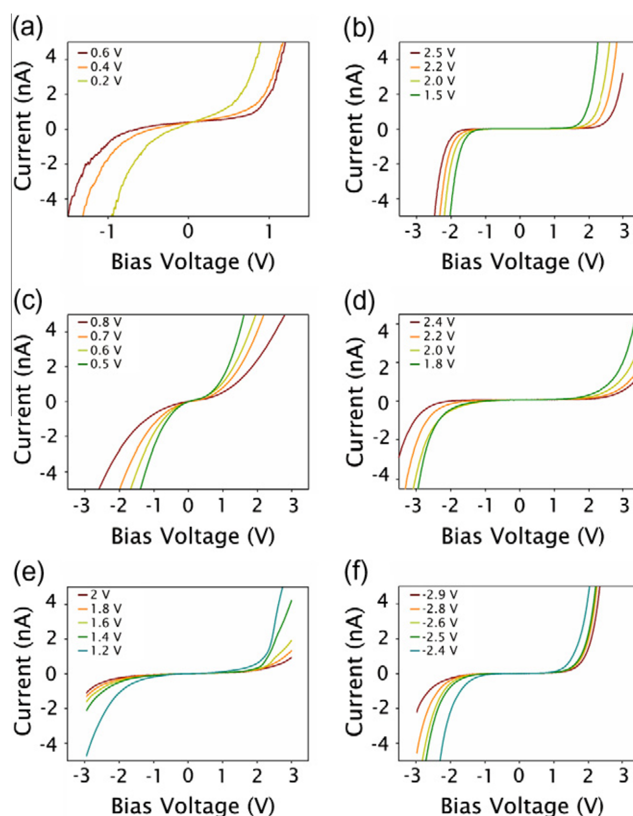

Fig. 7. *I*/*V* curves for bare substrates (left side) and C_{60} films (right side). All curves were taken at sample bias range from −3 V to +3 V and *I* = 1.0 nA. (a) Au, (b) C_{60}/Au, (c) HOPG, (d) C_{60}/HOPG, (e) SiO_x and (f) C_{60}/SiO_x.

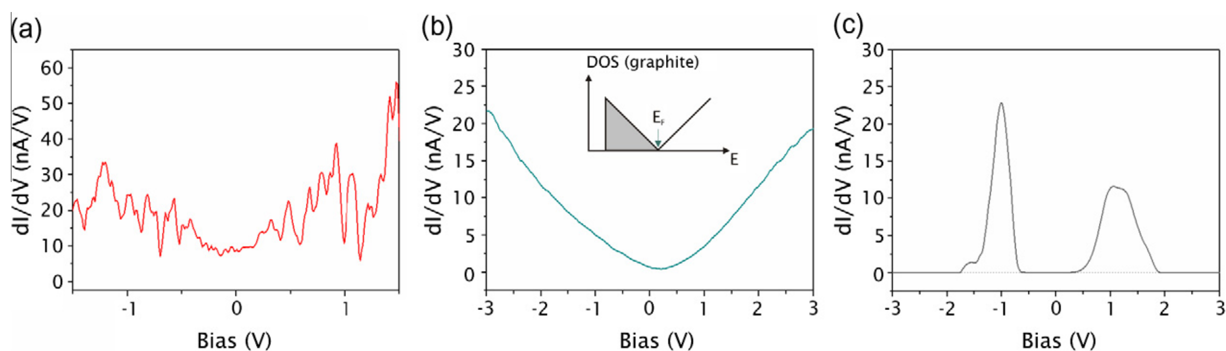

Fig. 8. The dI/dV curves measured for (a) Au (sample bias: 1 V), (b) HOPG (sample bias: 0.5 V) and (c) $Si0_x$/Si(1 0 0) (sample bias: 2 V) respectively. The current used in all spectra was 1.0 nA.

Fig. 9 shows *dI/dV* spectra for C_{60} films of different thicknesses prepared on SiO_x/Si(1 0 0). Our purpose was to address the electronic behavior of C_{60}/SiO_x/Si(1 0 0) system as the film thickness increases. Fig. 9(a) shows the STS spectrum for the 3 nm thick film (4 ML). The band gap obtained was 1.4 ± 0.1 eV with HOMO and LUMO at −1.0 and +0.4 eV, respectively. The Fermi level is shifted toward the LUMO band, which implies that there is a charge transfer from the SiO_x/Si(1 0 0) substrate to C_{60} consistent with the XPS data shown in Fig. 5c for the Si 2p signal, and in agreement with the results reported by Wang et al. for this system [17].

Fig. 9(b–d) summarizes STS data recorded for films thicker than 57 ML (40 nm). The gap values obtained are 1.6 ± 0.1, 1.6 ± 0.1 and 1.7 ± 0.1 eV, with HOMO energies of −0.7, −0.8 and −0.8 eV, and LUMO energies of 0.9, 0.8 and 0.9 eV for 40, 70 and 100 nm film-thicknesses, respectively. These results show that the gap is independent of thickness for smooth and thicker films and that their value correlates well with the gap for free C_{60} molecules [35], thus discarding the possibility that the film color could be caused by changes in the HOMO–LUMO position. In addition, we did not observe a LUMO shift towards the Fermi level (the spectra are symmetrical), suggesting that

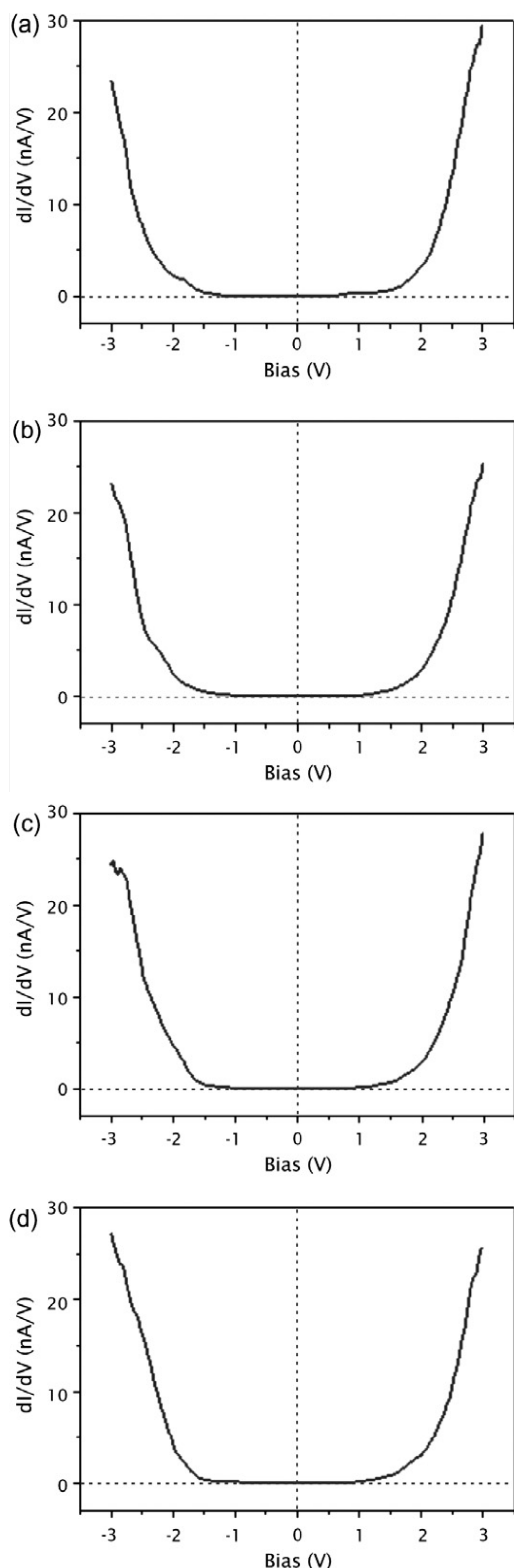

Fig. 9. STS spectra of $C_{60}/SiO_x/Si(1\,0\,0)$ for different film thicknesses: (a) 3 nm, (b) 40 nm, (c) 70 nm and (d) 100 nm. All curves were taken at sample bias of −3 V and current of 1.0 nA. The dashed line is shown to aid the gap visualization, and shows the symmetry with respect to the Fermi level.

there is no detectable charge transfer between Si and the outer C_{60} molecules, as expected for films with these thicknesses. In conclusion, we found that at high coverages (>57 ML) of C_{60} molecules deposited on $SiO_x/Si(1\,0\,0)$, the electronic characteristics of C_{60} films are very similar to those for C_{60}.

We have also tested the electronic properties of C_{60} films grown on Au and HOPG (Fig. 10). The clean Au and HOPG substrates exhibit ambient *dI/dV* curves typical of conducting materials (Fig. 8). However, after C_{60} deposition, the *dI/dV* plots show a semiconductor behavior with a gap of 1.6 ± 0.1 eV (HOMO = −0.8 eV and LUMO = +0.8 eV) and 2.5 ± 0.1 eV (HOMO = −1.3 eV and LUMO = +1.2 eV) for C_{60}/HOPG and C_{60}/Au, respectively. Both films have a thickness of 70 nm (100 ML of C_{60}) and show symmetrical behavior with respect to the Fermi level. The gap for C_{60}/HOPG is close to that obtained both for bulk C_{60}, and for the $C_{60}/SiO_x/Si$ film at the same coverage as above. In contrast, the gap of 2.5 ± 0.1 eV obtained for C_{60}/Au is higher than that for C_{60}/HOPG and Si substrate-surfaces, and comparable to those reported for single molecules and 1 ML of C_{60} deposited onto Au (gap values of 2.3–2.8 eV) [36–40]. The difference in the gap values measured for C_{60}/Au with respect to the C_{60} films

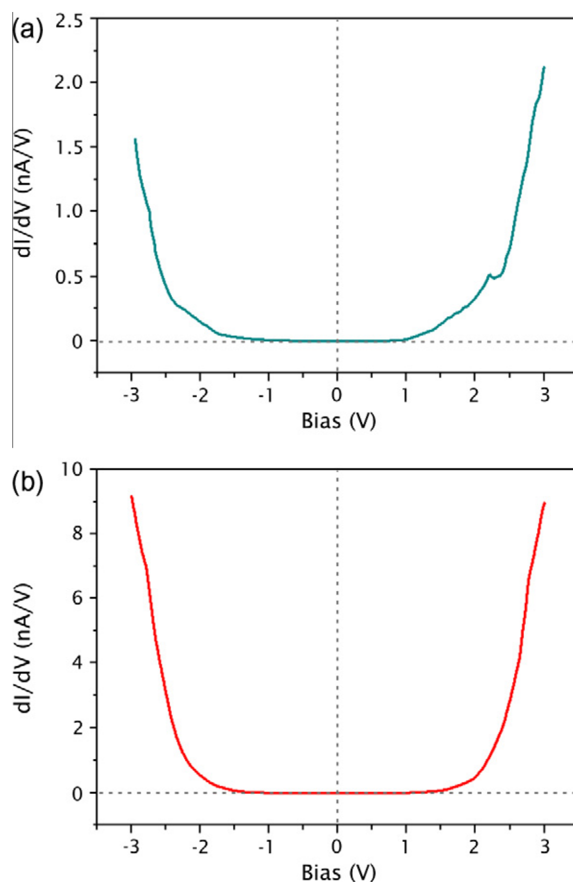

Fig. 10. STS spectra of (a) C_{60}/HOPG and (b) C_{60}/Au taken at sample bias of −3 V and current of 1.0 nA. The dashed line aids to visualize the gap of the film and shows the symmetry with respect to the Fermi level. The film thickness in both cases is 70 nm.

on the other substrates can, in principle, have multiple origins. While at first it is tempting to assign this value to charge transfer from Au to C_{60}, as for ultrathin C_{60} films, d*I*/d*V* curves are symmetric, essentially ruling out this possibility.

We next consider the structural differences in these films. Fernández-Torrente et al. [36] have shown that, for C_{60} films on Au(1 1 1), the gap obtained by STS changes in relation to the molecular environment. The differences in gap values measured for C_{60}/Au(1 1 1), with respect to the other substrates, seems to imply that the molecular environment for C_{60} on Au is different from the one in C_{60}/SiO_x/Si(1 0 0) and C_{60}/HOPG. If we take into account that the fullerene films were prepared simultaneously, in single evaporation experiments and with the same experimental setup, on all substrates, such preparation conditions imply that the mass of deposited fullerenes per unit surface area is the same for each sample, except perhaps during the very early stages of nucleation. However, once the steady growth state [51] is assumed to set in, (Fig. 4, $h \approx 30$ nm) the C_{60} films on Au (Fig. 4b) portray larger fullerene aggregates, and wider and deeper channels between them, than for example, on oxidized silicon (Fig. 4a). Bearing in mind that the mass of deposited fullerenes per unit surface area must be the same for each sample, under the same preparation conditions, the different morphologies could imply a local lowering of C_{60} density in the more extended grain-boundaries, resulting in a smaller number of C_{60} neighbors within the grain-boundaries. While this factor locally produces an increase in gap values, it is little likely that this change is detected by STS on an individual grain. Given that the initial thicknesses are comparable for all four kinds of substrates, these differences in gap values on Au could be a post-preparation effect, as we discuss below.

The fact that the electronic properties of the C_{60} films are not strongly modified by ambient conditions is at first surprising, particularly considering that their magnetic properties are modified. It has been reported that oxygen physisorbs (with a very small charge transfer) onto fullerene films, decreasing dramatically their conductivity [48]. Two distinct types of adsorbed oxygen were proposed [46]: oxygen incorporated at intergrain boundaries that rapidly quenches electronic transport, decreasing the intrinsic conductivity of C_{60} by one or two orders of magnitude, and oxygen at interstitial spaces of the C_{60} crystallites, resulting from slow diffusion, that lowers the conductivity of the material by about another two orders of magnitude. It has been shown, as well, that water diffusion is also important in C_{60} film degradation [49]. In principle, our results can be explained considering the kind of oxygen present in our C_{60} films and the different types of electronic measurements made by us and by other researchers. We propose that in our thicker film (where $d \approx h$) on Si, Au and HOPG, with nanometer sized grains, the dominant kind of physisorbed oxygen is at domain boundaries, so that it does not affect the molecular conductance measured by STS. Here we must recall that STS measures local properties resulting from electron transfer inside each nanometer-sized aggregate, and not the average properties of the films measured in other work, with non-local probes, where the contribution of domain boundaries is larger. In the case of C_{60}/Au, the larger grain boundary regions possibly enable a faster incorporation of oxygen at grain boundaries, that in turn could then interdiffuse into the grains, producing both swelling [45] and lowering of the conductivity, thus contributing to the increased gap of 2.5 eV observed for C_{60}/Au. In this case, the oxygen, initially incorporated into the more extended and deeper grain boundary regions of the film, can diffuse to interstitial C_{60} sites, thus effectively decreasing the local conductivity in the STS measurements. In summary, of the possible effects that could concurrently be responsible for the larger local band gap of C_{60} films on Au: charge transfer from the substrate to C_{60} molecules, as in ultra thin films; a local lowering of the grain-boundary packing density; and diffusion of oxygen to interstitial C_{60} sites; the latter is most probably the cause of the increase in the measured band gap on Au.

4. Conclusions

We have investigated the structure, chemical composition, magnetic and local electronic properties of thin C_{60} films (film thickness $\geqslant$ 4 ML) grown by sublimation on native silicon oxide, Au films, highly oriented pyrolytic graphite and glass, and subsequently exposed to ambient conditions. The films exhibit a structure consisting of nanometric aggregates, whose size increases with film thickness, irrespective of the substrate. Larger aggregates are systematically found on Au. The XPS data indicate no significant degradation of the C_{60} film although important amounts of oxygen are present in the films. The MFM data confirm that oxygen and light impact on the magnetic properties of C_{60}. In contrast, the STS measurements show little influence of ambient conditions on the local electronic properties. In fact, they are similar to those reported for ultrathin films grown and studied on the same substrates in UHV, i.e., in the absence of oxygen. For 4 ML of C_{60} on SiO_x, XPS data indicate the formation of a SiO_xC_y interface, in agreement with STS data showing charge transfer from SiO_x to C_{60}. The gap values for this film are close to those obtained in previous reports at lower coverages. On the other hand, thicker C_{60} films on SiO_x/Si and HOPG have gap values similar to those found for bulk C_{60}. In contrast, the electronic properties for C_{60} films on Au films show a larger gap value than those obtained on either HOPG or oxidized Si surfaces that, in our case, could be attributed to changes in the thin film structure, as a result of deep and extended domain boundaries. These extended boundaries on Au could facilitate the diffusion of oxygen to interstitial C_{60} sites, thereby increasing the band gap. The good adhesion and wear resistance of the thicker C_{60} films (40 nm < h < 100 nm), as well as the nearly constant local HOMO–LUMO gap on each substrate could become relevant for applications requiring manipulation, storage and operation under ambient conditions.

Acknowledgments

We acknowledge financial support from ANPCyT (Argentina, PICT06-621, PAE 22711, PICT-CNPQ 08-019), Gobierno de Canarias (ID20100152 ACIISI), MICIIN (Spain,

CTQ2008-06017/BQU), Spain, the National Autonomous University of Mexico (UNAM; grant DGAPA-IN100610), from the National Council of Science and Technology of Mexico (CONACYT; grant No. 127299) is greatly appreciated. O. A.-S. is grateful to the Posgrado en Ciencias Químicas UNAM and to CONACYT for a PhD fellowship.

References

[1] H.W. Kroto, J.R. Heath, S.C. O'Brien, R.F. Curl, R.E. Smalley, Nature 318 (1985) 162.
[2] W. Kratschmer, L.D. Lamb, K. Fostiropoulos, D.R. Huffman, Nature 347 (1990).
[3] S.A. Claridge, A.W. Castleman, S.N. Khanna, C.B. Murray, A. Sen, P.S. Weiss, ACS Nano 3 (2009).
[4] C.J. Brabec, S. Gowrisanker, J.J.M. Halls, D. Laird, S. Jia, S.P. Williams, Advanced Materials 22 (2010) 3839.
[5] L. Grausova, J. Vacik, V. Vorlicek, V. Svorcik, P. Slepicka, P. Bilkova, M. Vandrovcova, V. Lisa, L. Bacakova, Diamond and Related Materials 18 (2009) 578.
[6] D.M. Gruen, S. Liu, A.R. Krauss, J. Luo, X. Pan, Applied Physics Letters 64 (1994) 1502.
[7] D. Chen, R. Workman, D. Sarid, Surface Science 344 (1995).
[8] E. Radeva, V. Georgiev, L. Spassov, N. Koprinarov, S. Kanev, Sensors and Actuators B: Chemical 42 (1997) 11.
[9] J.-S. Shih, Y.-C. Chao, M.-F. Sung, G.-J. Gau, C.-S. Chiou, Sensors and Actuators B: Chemical 76 (2001) 347.
[10] N.-Y. Pan, J.-S. Shih, Sensors and Actuators B: Chemical 98 (2004) 180.
[11] H.-W. Chang, J.-S. Shih, Sensors and Actuators B: Chemical 121 (2007).
[12] R.M. Fleming, A.P. Ramirez, M.J. Rosseinsky, D.W. Murphy, R.C. Haddon, S.M. Zahurak, A.V. Makhija, Nature 352 (1991).
[13] H. Park, J. Park, A.K.L. Lim, E.H. Anderson, A.P. Alivisatos, P.L. McEuen, Nature 407 (2000).
[14] Y.Z. Li, M. Chander, J.C. Patrin, J.H. Weaver, L.P.F. Chibante, R.E. Smalley, Science 253 (1991) 429.
[15] T. Hashizume, X.D. Wang, Y. Nishina, H. Shinohara, Y. Saito, Y. Kuk, T. Sakurai, Japan Journal of Applied Physics 31 (1992) L880.
[16] H. Xu, D.M. Chen, W.N. Creager, Physical Review Letters 70 (1993) 1850.
[17] A.M. Rao, P. Zhou, K.A. Wang, G.T. Hager, J.M. Holden, Y. Wang, W.T. Lee, X.X. Bi, P.C. Ecklund, D.S. Cornett, M.A. Duncan, I.J. Amster, Science 259 (1993) 955.
[18] P. Moriarty, M.D. Upward, A.W. Dunn, Y.R. Ma, P.H. Beton, D. Teehan, Physical Review B 57 (1998) 362.
[19] K. Sakamoto, D. Kondo, Y. Ushimi, A. Kimura, A. Kakizaki, S. Suto, Surface Science 438 (1999) 248.
[20] J.I. Pascual, J. Gómez-Herrero, C. Rogero, A.M. Baró, D. Sánchez-Portal, E. Artacho, P. Ordejón, J.M. Soler, Chemical Physics Letters 321 (2000) 78.
[21] E.I. Altman, R.J. Colton, Surface Science 279 (1992) 49.
[22] A.J. Maxwell, P.A. Brühwiler, D. Arvanitis, J. Hasselström, M.K.-J. Johansson, N. Mårtensson, Physical Review B 57 (1998) 7312.
[23] C. Cepek, I. Vobornik, A. Goldoni, E. Magnano, G. Selvaggi, J. Kröger, G. Panaccione, G. Rossi, M. Sancrotti, Physical Review Letters 86 (2001) 3100.
[24] M. Grobis, X. Lu, M.F. Crommie, Physical Review B 66 (2002) 161408.
[25] A.W. Dunn, E.D. Svensson, C. Dekker, Surface Science 498 (2002).
[26] S. Suto, K. Sakamoto, T. Wakita, C.-W. Hu, A. Kasuya, Physical Review B 56 (1997) 7439.
[27] D. Kondo, K. Sakamoto, H. Takeda, F. Matsui, K. Amemiya, T. Ohta, W. Uchida, A. Kasuya, Surface Science 514 (2002) 337.
[28] L.-L. Wang, H.-P. Cheng, Physical Review B 69 (2004) 165417.
[29] H. Yu, J. Yan, Y. Li, W.S. Yang, Z. Gu, Y. Wu, Surface Science 286 (1993) 116.
[30] S. Suto, A. Kasuya, C.W. Hu, A. Wawro, K. Sakamoto, T. Goto, Y. Nishina, Thin Solid Films 281–282 (1996) 602.
[31] S. Szuba, R. Czajka, A. Kasuya, A. Wawro, H. Rafii-Tabar, Applied Surface Science 144–145 (1999) 648.
[32] D.J. Kenny, R.E. Palmer, Surface Science 447 (2000) 126.
[33] X. Yao, T.G. Ruskell, R.K. Workman, D. Sarid, D. Chen, Surface Science 366 (1996) L743.
[34] X. Yao, R.K. Workman, C.A. Peterson, D. Chen, D. Sarid, Applied Physics A: Materials Science & Processing 66 (1998) S107.
[35] H. Wang, C. Zeng, Q. Li, B. Wang, J. Yang, J.G. Hou, Q. Zhu, Surface Science 442 (1999) L1024.
[36] I. Fernández Torrente, K.J. Franke, J.I. Pascual, Journal of Physics: Condensed Matter 20 (2008) 184001.
[37] X. Lu, M. Grobis, K.H. Khoo, S.G. Louie, M.F. Crommie, Physical Review B 70 (2004) 115418.
[38] C. Rogero, J.I. Pascual, J. Gomez-Herrero, A.M. Baro, The Journal of Chemical Physics 116 (2002) 832.
[39] F. Schiller, M. Ruiz-Oses, J.E. Ortega, P. Segovia, J. Martinez-Blanco, B.P. Doyle, V. Perez-Dieste, J. Lobo, N. Neel, R. Berndt, J. Kroger, The Journal of Chemical Physics 125 (2006) 144719.
[40] G. Schull, N. Néel, M. Becker, J. Kröger, R. Berndt, New Journal of Physics 10 (2008).
[41] M. Nakaya, Y. Kuwahara, M. Aono, T. Nakayama, Small 4 (2008) 538.
[42] Y. Murakami, H. Suematsu, Pure and Applied Chemistry 68 (1996) 1463.
[43] A. Kumar, D.K. Avasthi, J.C. Pivin, Applied Physics Express 1 (2008) 125002.
[44] O.E. Kvyatkovskiia, I.B. Zakharovab, Fullerenes, Nanotubes, and Carbon Nanostructures 16 (2008) 574.
[45] T.L. Makarova, K.-H. Han, P. Esquinazi, R.R. Silva, Y. Kopelevich, I.B. Zakharova, B. Sundqvist, Carbon 41 (2003) 1575.
[46] B. Pevzner, A.F. Hebard, M.S. Dresselhaus, Physical Review B 55 (1997).
[47] M.S. Dresselhaus, G. Dresselhaus, R. Saito, Nanotechnology in carbon materials, in: G.L. Timp (Ed.), Nanotechnology, Springer-Verlag, New York, 1998, pp. 285–330.
[48] M. Foley, C. Ton-That, L. Kirkup, in: A. Barnhoorn, J.D. Fitz Gerald, I. Jackson, T.J. Senden (Eds.), 31st Annual Condensed Matter and Materials Meeting, Australian Institute of Physics, Wagga Wagga, 2007.
[49] H.B. Yang, Q.L. Song, C. Gong, C.M. Li, Solar Energy Materials and Solar Cells 94 (2010).
[50] A. Savitzky, M.J.E. Golay, Analytical Chemistry 36 (1964) 1627.
[51] P.C. dos Santos Claro, P.L. Schilardi, B. Blum, M.F. Castez, R.C. Salvarezza, Physical Review B 76 (2007).
[52] X.D. Wang, T. Hashizume, H. Shinohara, Y. Saito, Y. Nishina, T. Sakurai, Physical Review B 47 (1993) 15923.
[53] T.L. Makarova, B.B. Liu, B. Sundqvist, AIP Conference Proceedings 591 (2001).
[54] M. De Seta, N. Tomozeiu, D. Sanvitto, F. Evangelisti, Surface Science 460 (2000).
[55] C. Enkvist, S. Lunell, B. Sjogren, P.A. Bruhwiler, S. Svensson, The Journal of Chemical Physics 103 (1995) 6333.
[56] L. Charpentier, M. Balat-Pichelin, H. Glénat, E. Bêche, E. Laborde, F. Audubert, Journal of the European Ceramic Society 30 (2010).
[57] H. Yu, L.J. Webb, J.R. Heath, N.S. Lewis, Applied Physics Letters 88 (2006) 252111.
[58] K. Xue, H.P. Ho, J.B. Xu, Journal of Physics D: Applied Physics 40 (2007) 2886.
[59] J. Tersoff, D.R. Hamann, Physical Review B 31 (1985) 805.
[60] Z. Klusek, P. Kowalczyk, P. Byszewski, Vacuum 63 (2001) 145.
[61] Z.-Y. Yang, H.-M. Zhang, C.-J. Yan, S.-S. Li, H.-J. Yan, W.-G. Song, L.-J. Wan, Proceedings of the National Academy of Sciences 104 (2007) 3707.
[62] H. Ikegami, K. Ohmori, H. Ikeda, H. Iwano, S. Zaima, Y. Yasuda, Japanese Journal of Applied Physics 35 (1996) 1593.
[63] E. Nogales, B. Mendez, J. Piqueras, R. Plugaru, Semiconductor Science and Technology 16 (2001) 789.